

**ARTICLE**

Research on Human-Vehicle-Road Friendliness Based on Improved SH-GH-ADD Control

Yangyang Bao, Mingliang Yang, Haibo Huang, Liyuan Liu, Honglin Zhu and Weiping Ding*

School of Mechanical Engineering, Southwest Jiaotong University, Chengdu, 610031, China

*Corresponding Author: Weiping Ding. Email: dwp207@163.com

Received: 27 June 2023 Accepted: 08 September 2023 Published: 10 November 2023

ABSTRACT

The hub-driven virtual rail train is a novel urban transportation system that amalgamates the benefits of modern trams and buses. However, this system is plagued by issues such as decreased ride comfort and severe deformation of urban roads due to the increase in sprung mass and long-term rolling at the same position. To address these concerns and improve the human-vehicle-road friendliness of the virtual rail train, we propose an Improved Sky-Ground Hook and Acceleration-Driven Damper control (Improved SH-GH-ADD control) strategy for the semi-active suspension system. This control monitors the vibration acceleration signal of the unsprung mass in real-time and selects the mixed Sky-Hook and Acceleration-Driven Damper (SH-ADD) control or the mixed Ground-Hook and Acceleration-Driven Damper (GH-ADD) control based on the positive and negative values of the vibration acceleration of the unsprung mass. The Improved SH-GH-ADD control combines the advantages of SH-ADD control and GH-ADD control to achieve control of the sprung mass and unsprung mass in the full frequency band. Finally, through simulation and comparative analysis with traditional SH-ADD, GH-ADD, and mixed SH-GH control, we demonstrate the exceptional performance of the proposed algorithm.

KEYWORDS

SH control; GH control; ADD control; ride comfort; road friendliness

1 Introduction

The virtual rail train is a novel urban rail transit system that merges the characteristics of buses, trams, and light rail units to create a unique fusion of cars and trains, providing a solution to the road traffic pressure faced by small and medium-sized cities. In a study conducted on the virtual rail train in Zhuzhou, Hunan, and the intelligent rail in Yibin, Sichuan, it was observed that the running route of the train had caused severe permanent pavement deformation [1]. This deformation not only affects the quality and lifespan of the road but also leads to uneven pavement, ultimately impacting passenger comfort. Therefore, further research on human-vehicle-road friendliness of virtual rail trains is of great significance.

Considering the factors of energy consumption, control bandwidth, and system stability, semi-active suspension is considered to achieve the best results in terms of cost and performance. In the research of semi-active suspension control algorithm, the main focus is on controlling the vibration of the sprung mass or unsprung mass, with the aim of improving ride comfort and road friendliness. Some common



methods include robust control [2], Hybrid Control Algorithm Sliding Mode-PID [3], synovial control based on reference model [4], and optimal control [5], Nguyen proposed a fuzzy sliding mode ratio integral control method based on FSMPIF tuning to reduce the spring mass displacement and acceleration [6], and an adaptive fuzzy sliding mode proportional-integral-derivative method based on fuzzy tuning to reduce the body displacement and vibration acceleration [7]. In view of the real-time, engineering practicality, and simplicity of the algorithm, Sky-Hook (SH) control was first proposed by Karnopp et al. [8]. Ground-Hook (GH) control was proposed by Valášek et al. [9], and Acceleration-Driven Damper (ADD) control was widely used by Savaresi et al. [10].

Switched Sky-Hook (SH) and Acceleration-Driven Damper (ADD) have their respective advantages and disadvantages in suppressing the vibration of the sprung mass. Specifically, SH has a significant vibration control effect on the sprung mass in the low-frequency band (close to the inherent frequency domain of the sprung mass), but its vibration control effect on the sprung mass is not evident in the high-frequency band (beyond the inherent frequency domain of the sprung mass). In contrast, ADD's vibration control effect on the sprung mass is noticeable in the high-frequency band, but it is not evident in the low-frequency band (close to the inherent frequency domain of the sprung mass). Based on this situation, Savaresi et al. proposed a hybrid SH-ADD algorithm that combines the advantages of SH control and ADD control to achieve full-band suppression of sprung mass vibration, resulting in a good control effect [11]. Similarly, the switched Ground-Hook (GH) has a noticeable vibration control effect on the unsprung mass in the high-frequency band (exceeding the unsprung natural frequency domain), but its vibration control effect on the unsprung mass in the low-frequency band (close to the unsprung natural frequency domain) is not evident. Therefore, an ADD control strategy for unsprung mass control is proposed, combined with the reference ADD control. The characteristic of the ADD control is that the vibration control effect of the unsprung mass is noticeable in the low-frequency band (close to the unsprung natural frequency domain), while its vibration control effect is not evident in the high-frequency band (beyond the unsprung natural frequency domain). Based on this theory, the GH-ADD algorithm is proposed, which combines GH control and ADD control to achieve full-band suppression of unsprung mass vibration, resulting in a good control effect [12].

Due to the virtual rail train's intelligent operation on the established 'virtual track' and repeated rolling of the road, the damage to the road is more severe. Currently, the control strategies for ride comfort and road friendliness of virtual rail trains are limited. In contrast, in the field of heavy vehicles, mixed SH-GH control strategies are widely employed [13]. The control strategy combines SH and GH control by adjusting the weight co-efficient. However, in practical engineering applications, the fixed value of the weight co-efficient cannot be adjusted in real-time according to the vehicle operating conditions, resulting in different control effects under varying operating conditions. Considering the advantages and disadvantages of SH control and GH control, namely, the superior control effect of SH control on the sprung mass in the low-frequency band and the superior control effect of GH control on the unsprung mass in the high-frequency band, the simple combination of SH control and GH control cannot achieve the vibration suppression effect of the entire frequency band of the vehicle.

Given the aforementioned reasons, this paper proposes an Improved SH-GH-ADD control method. The control method achieves full-band control of the sprung mass by monitoring the vibration acceleration signal of the unsprung mass in real-time and utilizing the SH-ADD control when the unsprung acceleration is positive. Conversely, the selection of GH-ADD control also controls the unsprung mass in the full frequency domain. The proposed control strategy combines the advantages of SH-ADD control and GH-ADD control, which effectively reduces the vibration acceleration and tire dynamic.

The main contribution of this paper is to propose a damping control method based on the vibration acceleration of unsprung mass, which is used to control the vibration of sprung mass and unsprung mass. At the same time, the friendliness between human-vehicle-road is evaluated by various evaluation

indexes. In this study, the developed method achieves the control of the output damping force of the shock absorber by identifying specific parameters through the established multi-body vehicle dynamics. Then, a variety of evaluation indicators are used to compare and analyze various control strategies to evaluate the control effect of the model.

2 Evaluating Indicator

In order to conduct a comprehensive assessment of the impact of diverse control strategies on the overall performance of vehicles, it is imperative to take into account various factors such as human comfort, ride comfort, and road friendliness. Therefore, this research paper employs the environmental vibration dose value (eVDV) as a metric for evaluating human comfort. Moreover, the relationship between the weighted vibration level L_{wv} and weighted acceleration root mean square value and human subjective feeling is adopted as a measure of ride comfort. Furthermore, this paper introduces a predictive model of permanent deformation caused by repeated vehicle loads on roads as an evaluation index of road friendliness to determine the overall level of damage caused by vehicles to roads. Through the comprehensive analysis of the above evaluation indexes, the influence of various control strategies on the overall performance of the vehicle can be effectively evaluated.

2.1 Human Comfort Evaluation Index

The most important factor of environmental vibration on human health is the vibration frequency [14–17]. When the human body is affected by a certain frequency of environmental vibration, the degree of influence increases with the increase of vibration intensity. The natural frequency of the balance organ of the human body is in the range of 0.5~1.3 Hz. For the low-frequency vibration of 0~1 Hz, it can trigger the vestibular organ and central nervous system of the human body. The complex physiological and psycho-logical processes lead to the occurrence of motion sickness, which is manifested as the imbalance of the human body, vomiting, dizziness and other symptoms [18]. The frequency domain resonance range of the human body is 4~12.5 Hz, of which 4~8 Hz and 8~12.5 Hz are the resonance regions of the human internal organs and spinal system, respectively [19]. Therefore, long-term exposure to the vibration environment of the car will affect human health.

The objective evaluation of environmental vibration is mainly based on the quartic vibration dose value (VDV) and the estimated vibration dose value (eVDV) [20]. Because VDV is an evaluation dose with long detection duration and complicated calculation, it is used to evaluate the effect of high peak coefficient (peak factor greater than 9) vibration caused by excessive pulse on the human body, while eVDV is for continuous vibration with amplitude not changing with time and peak factor between 3 and 6. The eVDV value is slightly smaller than the VDV value, but the difference is very small and can be ignored [21]. The calculation formula of the quartic vibration dose value (VDV) and the estimated vibration dose value eVDV [22] is:

$$VDV = \left\{ \int_0^T [a_w(t)]^4 dt \right\}^{\frac{1}{4}} \quad (1)$$

$$eVDV = 1.4a_w T^{\frac{1}{4}} \quad (2)$$

$$a_w = \left[\sum_i (w_i a_i)^2 \right]^{\frac{1}{2}} \quad (3)$$

where: $a_w(t)$ is the instantaneous frequency weighted acceleration, m/s^2 ; a_w is frequency-weighted acceleration, m/s^2 ; T is the vibration exposure time in seconds; w_i is the weighting factor of the i th octave band given by ISO-2631:1997. a_i is the root mean square (rms) acceleration of the first octave band.

2.2 Vehicle Ride Comfort Evaluation Index

In order to better evaluate the ride comfort of the virtual track train of the new urban rail transit, this paper measures the vibration acceleration of the head car floor, and then converts it to the subjective feeling of passengers sitting on the seat according to the empirical formula, that is the vibration intensity at the floor is 1.4 times the vibration intensity on the seat [23], and the ride comfort of the virtual track train is evaluated by the weighted vibration level L_{aw} calculated by the converted seat vibration acceleration, in which the weighted vibration level L_{aw} is the weighted acceleration of the seat in a certain period of time. The formula of L_{aw} [19] is:

$$L_{aw} = 20 \log \frac{a_f}{1.4 \times 10^{-6}} \quad (4)$$

where: a_f is the weighted acceleration root mean square of the floor, m/s^2 .

Table 1 shows the relationship between the weighted vibration level L_{aw} and the root mean square value of the weighted acceleration and the subjective feelings of the person.

Table 1: The relationship between L_{aw} and seat vibration and human subjective feelings

Weighted acceleration root mean square of the seat (m/s^2)	The weighted vibration level L_{aw} (dB)	People's subjective feelings
< 0.315	110	No discomfort
0.315~0.63	110~116	Some discomfort
0.5~1.0	114~120	Quite uncomfortable
0.8~1.6	118~124	Uncomfortable
1.25~2.5	122~128	Very uncomfortable
> 2.0	126	Extremely uncomfortable

2.3 Road-Friendliness Criteria

In order to predict the overall damage degree of the road under repeated vehicle load, the empirical relationship between the permanent deformation of the granular layer and the subgrade and the number of load times and the compressive stress level is established [24]:

$$\delta_p = 18 \times 10^{-6} N^{0.813} (e^{B\sigma_v} - 1) \quad (5)$$

where: δ_p is the permanent deformation, mm; σ_v is vertical compressive stress, kPa; B is the coefficient related to the material properties; for South African standard materials, $\text{CBR} \geq 80\%$ of the granular layer, $B = 0.01$; $\text{CBR} \geq 45\%$ or 25% , $B = 0.017$; $\text{CBR} \geq 10\%$ or 7% , $B = 0.025$.

In order to calculate σ_v , this paper selects the axle load stress σ_v calculation formula [25], the expression is:

$$\sigma_v = Ar^m P_s^n h^{-2} \times 1000 \quad (6)$$

where: σ_v is the axial load stress, kPa; P_s is the static axle load of single axle-single wheel set, single axle-double wheel set or double axle-double wheel set, kN; r is the relative stiffness radius of concrete slab, m; h is the thickness of concrete slab, m; A , m , n are regression coefficients.

In this paper, $B = 0.01$, $A = 0.00180$, $m = 0.490$, $n = 0.881$, $r = 0.5$ m, $h = 0.52$ m.

Since P_s in Eq. (6) is the axle load of the vehicle, in order to obtain the dynamic force of the tire on the road surface during the movement of the virtual track train, the Eq. (6) is adjusted, that is:

$$\sigma_v = Ar^m(P_s + P_d)^n h^{-2} \times 1000 \quad (7)$$

where: P_d is the tire dynamic load.

Therefore, the permanent deformation prediction model of the overall damage degree of the vehicle load repeated on the road is:

$$\delta_p = 18 \times 10^{-6} N^{0.813} \left(e^{BAr^m(P_s+P_d)^n h^{-2} \times 1000} - 1 \right) \quad (8)$$

3 Vehicle System Dynamics Model

3.1 Dynamic Model of Hub-Driven Virtual Rail Train

The dynamic model of hub-driven virtual rail train is equivalent to a dynamic system with complete constraints. It is usually expressed by the differential-algebraic equations (DAEs) of index-3 [26], and its expression is:

$$\begin{cases} M(q, t)\ddot{q} + \Phi_q^T \lambda = F(\dot{q}, q, t) \\ \Phi(q, t) = 0 \end{cases} \quad (9)$$

where: $M \in R^{n \times n}$ is the mass matrix of the components; $q \in R^n$ is a generalized coordinate; $\lambda \in R^n$ is a Lagrange multiplier; Φ is the constraint equation of generalized coordinate q ; Φ_q is the Jacobi matrix of the constraint equation; $F \in R^n$ is a generalized force vector.

By solving the first and second derivatives of the constraint equation $\Phi(q, t) = 0$, the differential-algebraic equations of index-2 and index-1 can be obtained, respectively:

$$\begin{cases} M(q, t)\ddot{q} + \Phi_q^T \lambda = F(\dot{q}, q, t) \\ \Phi_q \dot{q} + \Phi_t = 0 \end{cases} \quad (10)$$

$$\begin{cases} M(q, t)\ddot{q} + \Phi_q^T \lambda = F(\dot{q}, q, t) \\ \Phi_q \ddot{q} + (\Phi_q \dot{q})_q \dot{q} + 2\Phi_{qt} \dot{q} + \Phi_{tt} = 0 \end{cases} \quad (11)$$

As shown in Fig. 1, the 1/4 vehicle model of the virtual rail train adopts a double wishbone suspension, which is mainly connected by a spherical hinge joint, a cylindrical pair, a revolute pair and a universal joint, and has a certain dynamic performance through the damping force of the shock absorber, the stiffness of the spring and the bushing. The revolute joint limits its degree of freedom to 1 and can only rotate in one plane. For example, Fig. 2 is a planar double-link mechanism with two revolute joints. Assuming that the system is only affected by gravity, the gravitational acceleration is $g = 9.81 \text{ m/s}^2$, and the system state variable $q = (x_1, y_1, \theta_1, x_2, y_2, \theta_2)$, then the dynamic differential algebraic equation of the system [27] is:

$$\begin{bmatrix} M & \Phi_q^T \\ \Phi_q & 0 \end{bmatrix} \begin{bmatrix} \ddot{q} \\ \lambda \end{bmatrix} = \begin{bmatrix} F \\ -(\Phi_q \dot{q})_q \dot{q} \end{bmatrix} \quad (12)$$

where: generalized force vector $F = (0, -m_1 g, 0, 0, -m_2 g, 0)$, generalized mass matrix $M = \text{diag}(m_1, m_1, J_1, m_2, m_2, J_2)$, connecting rod moment of inertia $J_1 = \frac{1}{12} m_1 L_1^2, J_2 = \frac{1}{12} m_2 L_2^2$.

The cylindrical pair limits its degree of freedom to 2, can rotate in a plane and can move in its axial direction. For example, Fig. 3 is a mechanism with a cylindrical pair. Assuming that the system is only affected by gravity, the gravity acceleration is $g = 9.81 \text{ m/s}^2$, and the system state variable

$q = (x_1, y_1, z_1, \theta_1)$, the differential-algebraic equation of system dynamics is:

$$\begin{bmatrix} M & \Phi_q^T \\ \Phi_q & 0 \end{bmatrix} \begin{bmatrix} \ddot{q} \\ \dot{\lambda} \end{bmatrix} = \begin{bmatrix} F \\ -(\Phi_q \dot{q})_q \dot{q} \end{bmatrix} \quad (13)$$

where: generalized force vector $F = (0, 0, -m_1g, 0)$, generalized mass matrix $M = \text{diag}(m_1, m_1, m_1, J_1)$, connecting rod moment of inertia $J_1 = \frac{1}{12}m_1L_1^2$.

The spherical hinge joint limits its degree of freedom to 3 and can rotate in three axial directions. For example, Fig. 4 is a mechanism with a spherical hinge joint, where H is the axis of the rod m_1 , H_{xy} , H_{xz} and H_{yz} are the projections of H to XY plane, XZ plane and YZ plane, respectively. Suppose that the system is only affected by gravity, the gravity acceleration is $g = 9.81 \text{ m/s}^2$, the system state variable $q = (x_1, y_1, z_1, \theta_1, \theta_2, \theta_3)$, the differential-algebraic equation of the system dynamics of the spherical hinge joint is:

$$\begin{bmatrix} M & \Phi_q^T \\ \Phi_q & 0 \end{bmatrix} \begin{bmatrix} \ddot{q} \\ \dot{\lambda} \end{bmatrix} = \begin{bmatrix} F \\ -(\Phi_q \dot{q})_q \dot{q} \end{bmatrix} \quad (14)$$

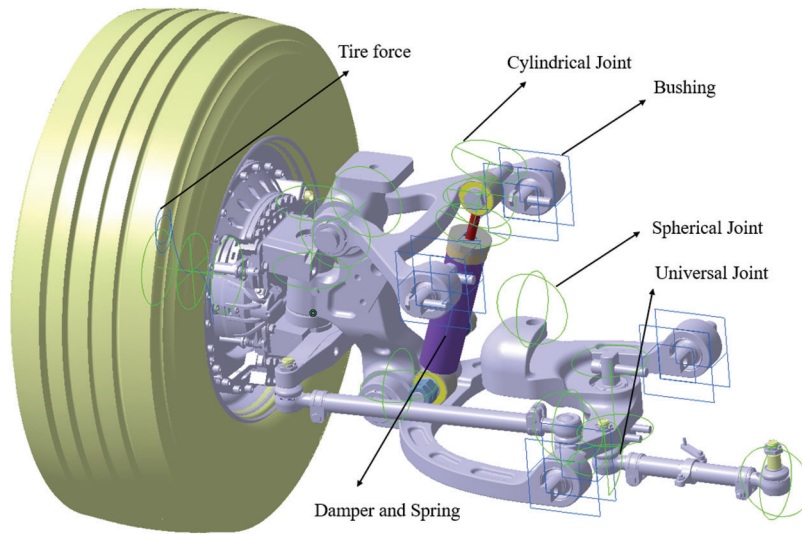


Figure 1: Virtual rail train 1/4 vehicle model

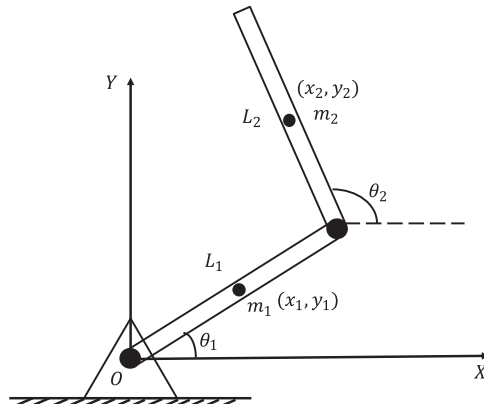


Figure 2: Planar double-link mechanism

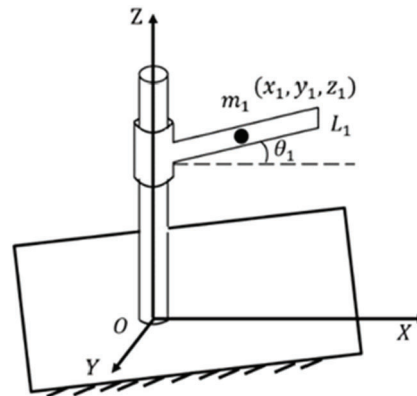


Figure 3: Mechanisms with cylindrical pairs

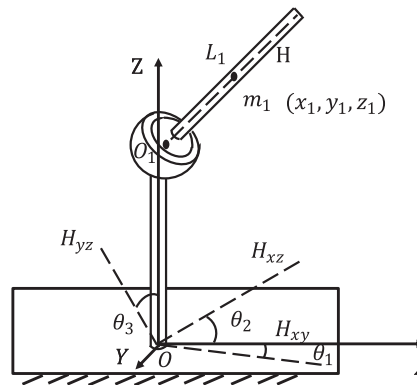


Figure 4: Mechanism with spherical hinge joint

The universal joint limits its degree of freedom to 2 and can rotate in two axial directions. For example, Fig. 5 is a mechanism with a universal joint, where H is the axis of the rod m_1 , H_{xy} and H_{xz} are the projections of H to the XY plane and the XZ plane, respectively. Suppose that the system is only affected by gravity, the gravity acceleration is $g = 9.81 \text{ m/s}^2$, the system state variable $q = (x_1, y_1, z_1, \theta_1, \theta_2)$, the differential-algebraic equation of the system dynamics of the universal joint is:

$$\begin{bmatrix} M & \Phi_q^T \\ \Phi_q & 0 \end{bmatrix} \begin{bmatrix} \ddot{q} \\ \lambda \end{bmatrix} = \begin{bmatrix} F \\ -(\Phi_q \dot{q})_q \dot{q} \end{bmatrix} \tag{15}$$

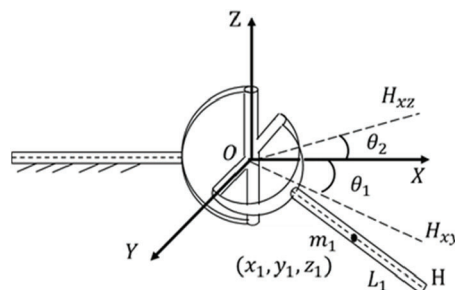


Figure 5: Mechanisms with universal joints

where: generalized force vector $F = (0, 0, -m_1g, 0, 0)$, generalized mass matrix $M = \text{diag}(m_1, m_1, m_1, J_1, J_1)$, connecting rod moment of inertia $J_1 = \frac{1}{12}m_1L_1^2$.

The Spring-Damping force system [28] is shown in Fig. 6, object I and object J are connected by Spring-Damper (SD), and the connection points are p^i and p^j . The generalized coordinates of the two objects relative to the global coordinate system at the current time are:

$$q_i = (R_i^T \quad \theta_i^T)^T \quad (16)$$

$$q_j = (R_j^T \quad \theta_j^T)^T \quad (17)$$

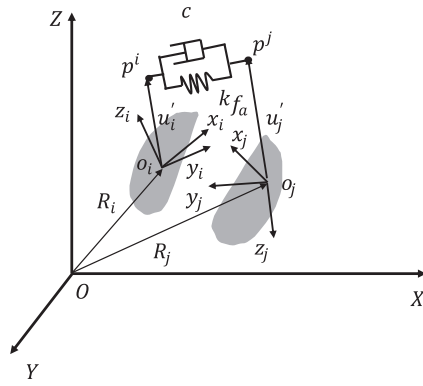


Figure 6: Spring-damping force system

The generalized speed is:

$$\dot{q}_i = (\dot{R}_i^T \quad \dot{\theta}_i^T)^T \quad (18)$$

$$\dot{q}_j = (\dot{R}_j^T \quad \dot{\theta}_j^T)^T \quad (19)$$

where: $R_i \in R^{3 \times 1}$ and $R_j \in R^{3 \times 1}$ represent the projection of the origin of the local coordinate system fixed on object I and object J relative to the vector of the global coordinate system in the global coordinate system. θ_i and θ_j represent the attitude angles of the local coordinate system relative to the global coordinate system, respectively.

The force of SD is always along the line of p^i and p^j , and its size is:

$$F_s = ks + c\dot{s} \quad (20)$$

where: k is the spring stiffness; c is the damping coefficient of the shock absorber; s is the deformation of the spring.

The array of the force acting on object I and object J in the global coordinate system is:

$$F_s^i = -F_s \hat{s} \quad (21)$$

$$F_s^j = F_s \hat{s} \quad (22)$$

where: $F_s^i \in R^{3 \times 1}$, $F_s^j \in R^{3 \times 1}$; $\hat{s} \in R^{3 \times 1}$ is the unit vector.

The virtual work done by SD is:

$$\delta W = (F_s^i)^T \delta R_{p_i} + (F_s^j)^T \delta R_{p_j} \quad (23)$$

$$\delta R_{p_i} = (E - A_i u_i' G_i) \delta q_i \quad (24)$$

$$\delta R_{p_j} = (E - A_j u_j' G_j) \delta q_j \quad (25)$$

where: E is expressed as a unit matrix of order 3; $A_i \in R^{3 \times 3}$ and $A_j \in R^{3 \times 3}$ are the direction cosine matrices corresponding to θ_i and θ_j .

Then the relationship between generalized force vectors $Q_{ei} \in R^{N \times 1}$ and $Q_{ej} \in R^{N \times 1}$ of SD and virtual work is:

$$\delta W = Q_{ei}^T \delta q_i + Q_{ej}^T \delta q_j \quad (26)$$

Bring Eqs. (21)~(22) and (24)~(25) into Eq. (23) and compare them with Eq. (26). The generalized force vectors acting on objects I and J are:

$$Q_{ei} = (E - A_i u_i' G_i)^T F_s^i = -(E - A_i u_i' G_i)^T (F_s \times \hat{s}) \quad (27)$$

$$Q_{ej} = (E - A_j u_j' G_j)^T F_s^j = -(E - A_j u_j' G_j)^T (F_s \times \hat{s}) \quad (28)$$

Based on the principle of DAEs, the mechanism of various kinematic pairs and elastic elements in the 1/4 vehicle dynamics model is analyzed. Because the semi-active control algorithm tends to 1/4 suspension model, it is easier to study and analyze the characteristics of the algorithm by using 1/4 suspension model, but it cannot fully reflect the complex environment and the nonlinear characteristics of the vehicle itself. Therefore, in order to improve the transmission efficiency between components, this paper establishes a hub-driven virtual rail train dynamics model based on a multi-body dynamics software, as shown in Fig. 7. As shown in Table 2, except that the ‘minimum/maximum damping coefficient‘ comes from experience, the remaining parameters are measured by the virtual rail train.

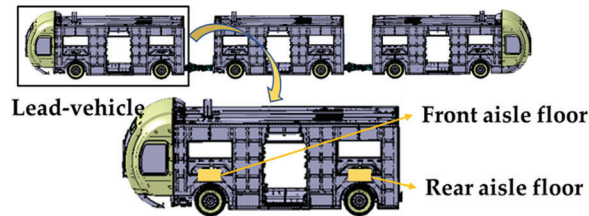


Figure 7: Dynamic model of hub-driven virtual rail train

3.2 Dynamic Model of Hub-Driven Virtual Rail Train

In order to verify the validity and correctness of the multi-body dynamics model, simulation and experiment are used to verify each other. Due to the limited conditions in the development and design stage, the test condition is that the vehicle is driven on the asphalt pavement (Grade B pavement) at a speed of 15 km/h under full load (as shown in Fig. 8). The vibration acceleration signals at the corresponding points of the front aisle floor and the rear aisle floor of the lead-vehicle are measured by the acceleration sensor, as shown in Figs. 7 and 9, and the respective acceleration frequency domain signals are obtained.

Table 2: Vehicle model parameters

Parameter	Parameter value
Lead-vehicle sprung mass (kg)	18245
Middle car sprung mass (kg)	18000
Unsprung mass (kg)	7044
Wheel track (m)	2.65
Wheel base (m)	5.2
Body center of gravity height (m)	2.31
Tire radius (m)	0.534
Tire stiffness ($N \cdot m^{-1}$)	1155000
Passive suspension stiffness ($N \cdot m^{-1}$)	130000
Passive suspension damping coefficient ($N \cdot s \cdot m^{-1}$)	10000
The minimum damping coefficient c_{min} ($N \cdot s \cdot m^{-1}$)	3330
The maximum damping coefficient c_{max} ($N \cdot s \cdot m^{-1}$)	30000

**Figure 8:** Vehicle track path**Figure 9:** Acceleration sensor on floor of front aisle and rear aisle

As shown in Figs. 10 and 11, the vibration acceleration frequency domain signals at the corresponding points of the front aisle and the rear aisle of the lead-car are simulated and tested. Table 3 shows the comparison between the simulation results and the test results.

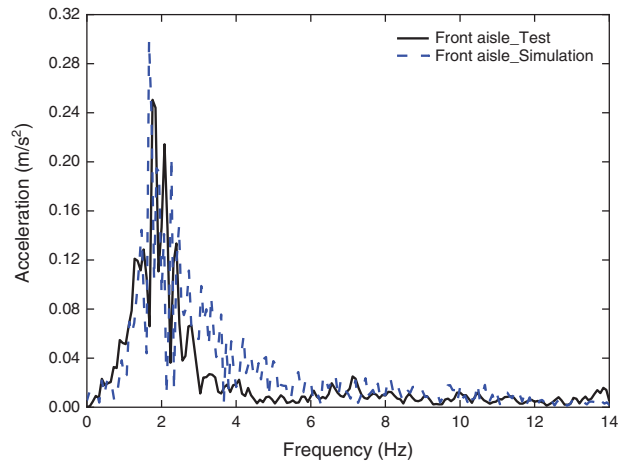


Figure 10: Frequency domain response at the front aisle floor of the lead-vehicle

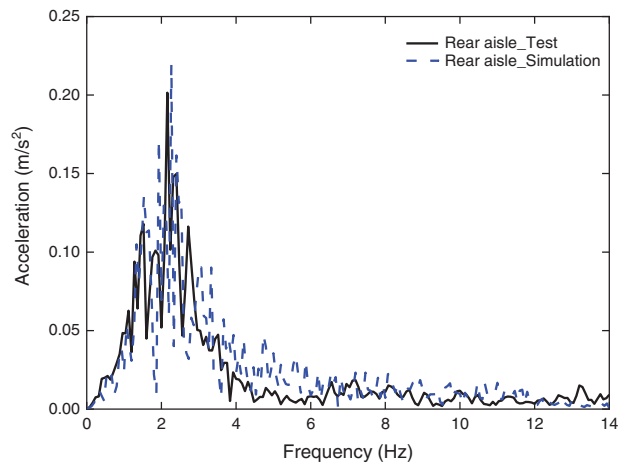


Figure 11: Frequency domain response at the rear aisle floor of the lead-vehicle

Table 3: Simulation results and test results

Parameter	Front aisle floor			Front aisle floor		
	Test	Simulation	Precision	Test	Simulation	Precision
Maximum peak frequency point (Hz)	1.76	1.67	94.9%	2.16	2.27	95.2%
Maximum crest (m/s^2)	0.25	0.29	86.2%	0.20	0.22	90.9%

As shown in [Table 3](#), the simulation results are basically consistent with the experimental results, but there are some differences. These differences are mainly due to the following reasons:

1. The B-level road surface used in the simulation is generated by simulating random road roughness, which is not obtained by real measurement, so there is a certain difference between the road surface and the actual test.

2. In the simulation process, the frame is only regarded as a rigid body without considering the flexible treatment. However, in practice, the large bus wheelbase is larger, resulting in lower frame stiffness.
3. There are also some differences between the tires used in the simulation and the actual tires.

In general, the accuracy of experimental data and simulation data is maintained above 86% from the perspective of peak value and peak frequency, which proves that the established dynamic model has high validity and correctness. However, it should be noted that the above differences may have an impact on the results.

4 Improved SH-GH-ADD Control Strategy

4.1 Passive Suspension 1/4 Model

The classical damping control is aimed at the single-freedom vibration system, which is more suitable for the vertical vibration control of the 1/4 vehicle model with two degrees of freedom. At present, the mainstream idea of vehicle damping control is to promote and apply the 1/4 damping suspension model from the physical point of view. Therefore, it is necessary to introduce and analyze the 1/4 suspension model. The 1/4 model of vehicle suspension system is shown in Fig. 12.

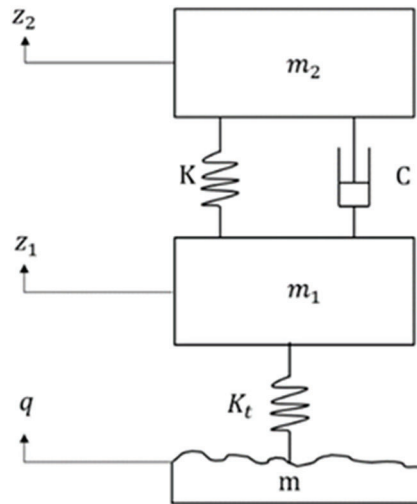


Figure 12: Suspension system 1/4 model

According to the Lagrange equation, the differential equation of motion of the 1/4 suspension system of the virtual track train is established:

$$m_2 \ddot{z}_2 = -k(z_2 - z_1) - c(\dot{z}_2 - \dot{z}_1) \quad (29)$$

$$m_1 \ddot{z}_1 = -k(z_1 - z_2) - c(\dot{z}_1 - \dot{z}_2) - k_t(z_1 - q) \quad (30)$$

$$m \ddot{q} = -k_t(q - z_1) \quad (31)$$

where: m_1 and m_2 are unsprung and sprung mass, respectively; m is the hypothetical pavement mass; q , z_1 and z_2 are road roughness, unsprung and sprung displacement, respectively; k is the suspension stiffness; c is suspension damping; k_t is the tire stiffness.

4.2 Classical Damping Control

Classical damping control includes SH control, GH control and ADD control [29]. SH is assumed that there is a damper connected to the reference position (sky) and the vehicle body to suppress the body vibration caused by the road roughness excitation [30,31]. For the switch-type SH control, the control principle is:

$$C_{in}(SH) = \begin{cases} c_{max}, & \dot{z}_2(\dot{z}_2 - \dot{z}_1) > 0 \\ c_{min}, & \dot{z}_2(\dot{z}_2 - \dot{z}_1) < 0 \end{cases} \quad (32)$$

where: $C_{in}(SH)$ is the SH damping coefficient: c_{max} is the maximum damping coefficient provided by the shock absorber; c_{min} is the minimum damping coefficient provided by the shock absorber.

GH is assumed that there is a damper connected to the reference position (ground) and unsprung mass to suppress the unsprung mass vibration caused by road roughness excitation. For the switch-type GH control, the control principle is:

$$C_{in}(GH) = \begin{cases} c_{min}, & \dot{z}_1(\dot{z}_2 - \dot{z}_1) > 0 \\ c_{max}, & \dot{z}_1(\dot{z}_2 - \dot{z}_1) < 0 \end{cases} \quad (33)$$

where: $C_{in}(GH)$ is the damping coefficient of the GH.

In the traditional vehicle suspension control, ADD aims to suppress the body acceleration. For the switching ADD control, the control principle is:

$$C_{in}(ADD) = \begin{cases} c_{max}, & \ddot{z}_2(\dot{z}_2 - \dot{z}_1) > 0 \\ c_{min}, & \ddot{z}_2(\dot{z}_2 - \dot{z}_1) < 0 \end{cases} \quad (34)$$

where: $C_{in}(ADD)$ is the damping coefficient of the ADD.

SH is widely used in automobile suspension. The goal is to suppress the body acceleration \ddot{z}_2 near the natural frequency of the sprung mass, therefore, the control effect of the sprung mass is good, but the control of the unsprung mass is poor. GH is widely used in the suspension of heavy vehicles. The goal is to suppress the unsprung mass acceleration \ddot{z}_1 above the natural frequency of the unsprung mass, therefore, the control effect of the unsprung mass is good, but the control of the sprung mass is poor. The acceleration damping strategy is generally used in conjunction with the ceiling control. The ADD control aims to suppress the body acceleration \ddot{z}_2 above the natural frequency of the sprung mass, therefore, the control effect of the sprung mass is good, but the control of the unsprung mass is poor.

4.3 Mixed SH-GH Control

SH control and GH control are complementary in the control effect of vertical vibration of vehicles. SH control is mainly the control of sprung mass vibration, while GH control is mainly the control of unsprung mass vibration. Mixed SH-GH control [32] connects SH control with GH control by adjusting the value of parameter u , and realizes the proportion of sprung and unsprung mass control by adjusting the value of u . The control principle of Mixed SH-GH control is shown in equation, where the value range of u is $[0, 1]$. When $u = 1$, it is pure ceiling control. When $u = 0$, it is pure floor control. When u is between 0 and 1, it combines the characteristics of SH and GH. The damping force generated by Mixed SH-GH control is:

$$f_{SH-GH} = uc_{sky}\dot{z}_2 + (1 - u)c_g\dot{z}_1 \quad (35)$$

where: f_{SH-GH} is the damping force of the mixed SH-GH; u is the weight coefficient value, $u = 0.3$ in this paper; c_{sky} is the SH damping coefficient; c_g is the damping coefficient of the GH.

The control of the mixed SH-GH combines the advantages of the SH control and the GH control. However, because SH control has a better vibration suppression effect on the sprung mass near the natural frequency of the sprung mass, the GH control has a better vibration suppression effect on the unsprung mass above the natural frequency of the unsprung mass; Once the engineering application is carried out, the weight coefficient value will not change in real time with the vehicle operating conditions, so the control effect is different under different operating conditions; As shown in Eq. (35), in theory, the shock absorber cannot provide two damping coefficients at the same time, that is, c_{sky} and c_g cannot exist at the same time; the mixed sky and ground control is a continuously adjustable control, while the sky and ground control are both switch-type control.

4.4 Improved SH-GH-ADD Control Strategy

At present, there are still some defects in the classical damping control and mixed SH-GH control in terms of human-vehicle-road friendliness, that is, it is impossible to reasonably select control strategies for the vibration frequency of human body and vehicle to improve human-vehicle-road friendliness. Therefore, two new control strategies, SH-ADD control and GH-ADD control are proposed. The control principles are as follows:

$$C_{in}(SH - ADD) = \begin{cases} C_{in}(ADD), & \ddot{z}_2^2 - \beta_2 \dot{z}_2^2 \geq 0 \\ C_{in}(SH), & \ddot{z}_2^2 - \beta_2 \dot{z}_2^2 < 0 \end{cases} \quad (36)$$

where: $C_{in}(SH - ADD)$ is the SH-ADD damping coefficient. β_2 is the frequency (circular frequency) switching coefficient.

In order to reasonably determine β_2 , the amplitude-frequency characteristics of the sprung mass are analyzed. The transfer function between the sprung mass and the road input is:

$$H_{z_2} = \frac{(ck_t)s + k_t k}{(m_2 m_1)s^4 + (cm_1 + cm_2)s^3 + (m_2 k + m_1 k + m_2 k_t)s^2 + k_t k} \quad (37)$$

$$\begin{cases} \omega_1 = \frac{1}{2\pi\sqrt{2m_1 m_2}} \sqrt{m_1 m_2 (m_2 k_t + 2m_2 k + 2m_1 k - \alpha)} \\ \omega_2 = \frac{1}{2\pi} \sqrt{\frac{k_t}{m_1}} \\ \omega_3 = \frac{1}{2\pi\sqrt{2m_1 m_2}} \sqrt{m_1 m_2 (m_2 k_t + 2m_2 k + 2m_1 k + \alpha)} \end{cases} \quad (38)$$

where:

$$\alpha = \sqrt{4m_1^2 k^2 - 4m_1 k m_2 k_t + 8m_2 k^2 m_1 + m_2^2 k_t^2 + 4m_2^2 k k_t + 4m_2^2 k^2} \quad (39)$$

As shown in Fig. 13, in the low frequency band, if the damping is increased, it is helpful to reduce the amplitude of the sprung mass, while in the middle and high frequency bands, the result is opposite. If the damping is increased, the amplitude of the sprung mass will increase. Among them, w_1 separates the low frequency band from the middle and high frequency bands, and the frequency range of segmentation is the widest, so $\beta_2 = 2\pi w_1$.

GH-ADD control is to realize the control of unsprung mass in the whole frequency band. Referring to ADD control, ADD control suitable for unsprung mass control is proposed, which combines the advantages of GH control. It is characterized by ADD control in low frequency (near the natural frequency domain of unsprung mass) and GH control in high frequency (above the natural frequency of unsprung mass). GH-

ADD control can suppress the vibration of unsprung mass in the whole frequency band. The principle of GH-ADD control is as follows:

$$C_{in}(GH - ADD) = \begin{cases} C_{in}(GH), & \ddot{z}_1^2 - \beta_1 \dot{z}_1^2 \geq 0 \\ C_{in}(ADD), & \ddot{z}_1^2 - \beta_1 \dot{z}_1^2 < 0 \end{cases} \quad (40)$$

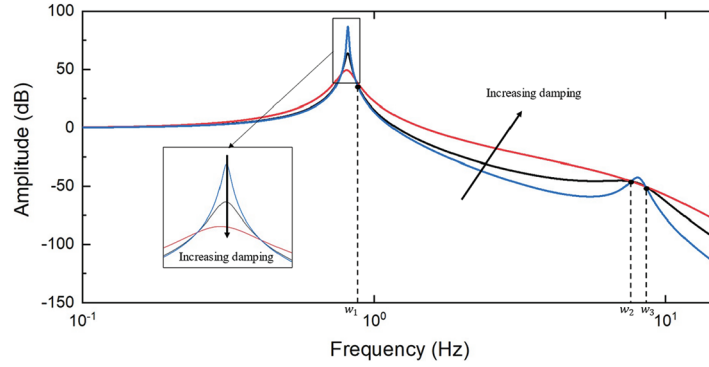


Figure 13: Amplitude-frequency characteristics of sprung mass

Aiming at the control of unsprung mass, an ADD control similar to Eq. (34) is proposed. The ADD control rules in GH-ADD control are as follows:

$$C_{in}(ADD) = \begin{cases} c_{min}, & \ddot{z}_1(\dot{z}_2 - \dot{z}_1) > 0 \\ c_{max}, & \ddot{z}_1(\dot{z}_2 - \dot{z}_1) < 0 \end{cases} \quad (41)$$

where: $C_{in}(GH - ADD)$ is the GH-ADD damping coefficient. β_1 is the frequency (circular frequency) switching coefficient.

In order to reasonably determine β_1 , the amplitude-frequency characteristics of unsprung mass are analyzed. The transfer function between the unsprung mass and road input is:

$$H_{z_1} = \frac{(m_2 k_t) s^2 + (c k_t) s + k_t k}{(m_2 m_1) s^4 + (c m_1 + c m_2) s^3 + (m_2 k + m_1 k + m_2 k_t) s^2 + k_t k} \quad (42)$$

$$\omega_4 = \frac{1}{2\pi} \sqrt{\frac{k_t}{m_2 + m_1}} \quad (43)$$

As shown in Fig. 14, in the low frequency band, if the damping is increased, it is not conducive to reducing the amplitude of the unsprung mass, while in the middle and high frequency bands, the result is opposite. If the damping is increased, the amplitude of the unsprung mass will be reduced. Among them, w_4 separates the low frequency band from the middle and high frequency bands, and the frequency range of segmentation is the widest, so $\beta_1 = 2\pi w_4$.

Although SH-ADD control and GH-ADD control can achieve full-band vibration suppression, they can only control the sprung mass or unsprung mass, and cannot achieve full-band vibration suppression of sprung and unsprung mass.

To reduce the force of the vehicle on the road, it is necessary to reduce the vibration acceleration of the sprung and unsprung. Since the inertia force of the unsprung mass will directly act on the ground, the inertia force of the unsprung mass can be derived from the 1/4 model of the 4.1 suspension system:

$$F_1 = m_1 \ddot{z}_1 - m_2 \ddot{z}_2 \quad (44)$$

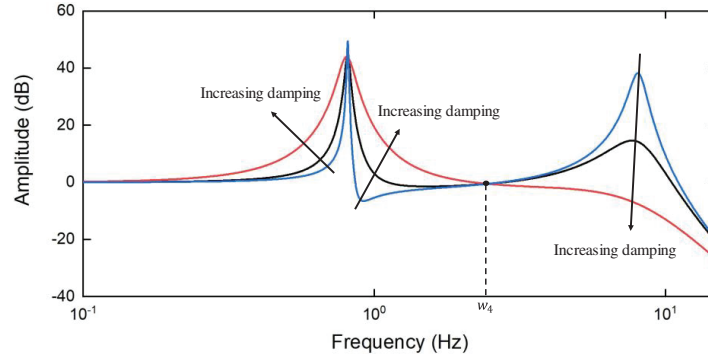


Figure 14: Amplitude-frequency characteristics of unsprung mass

It can be seen that when the vibration acceleration \ddot{z}_1 of the unsprung mass and the vibration acceleration \ddot{z}_2 of the sprung mass decrease, the inertia force $|F_1|$ of the unsprung mass can be reduced. According to Newton second law, when the acceleration of the unsprung mass is negative, the force of the tire on the ground increases, and at this time, the focus should be on protecting the road surface; when the acceleration of the unsprung mass is positive, the force of the tire on the ground is weakened, and the protection of the road surface is less important, which in turn should protect the passengers. Therefore, based on this principle, this paper proposes an improved SH-GH-ADD control strategy, as shown in Fig. 15. The control principle is that when the unsprung mass acceleration \ddot{z}_1 is negative, the GH-ADD control is adopted to realize the control of the unsprung mass in the whole frequency band; when the unsprung mass acceleration \ddot{z}_1 is positive, the SH-ADD control is used to realize the control of the sprung mass in the full frequency band. The control principle of improved SH-GH-ADD control is as follows:

$$C_{in}(\text{Improved SH} - \text{GH} - \text{ADD}) = \begin{cases} C_{in}(\text{SH} - \text{ADD}), & \ddot{z}_1 > 0 \\ C_{in}(\text{GH} - \text{ADD}), & \ddot{z}_1 < 0 \end{cases} \quad (45)$$

where: $C_{in}(\text{Improved SH} - \text{GH} - \text{ADD})$ is the improved SH-GH-ADD control damping coefficient.

5 Analysis of Vehicle Simulation Results

In order to verify the superiority of the improved SH-GH-ADD control over the SH-ADD control, the GH-ADD control and mixed SH-GH control, this study used the constructed virtual track train to carry out simulation analysis and verification of human comfort, ride comfort and road friendliness. The design speed of the virtual rail train is 70 km/h, the actual running speed is 60 km/h, and the urban road surface grade is B. Under this condition, we studied the influence of the improved SH-GH-ADD control strategy on the human-vehicle-road friendliness through simulation analysis. Considering that the three carriages of the virtual rail train have certain similarity and a large amount of data, this paper only shows the data of the lead-vehicle for analysis.

5.1 Human Comfort Analysis

In order to determine whether the quartic vibration dose value (VDV) or the estimated vibration dose value (eVDV) is used for the objective evaluation of environmental vibration in the comfort evaluation index 2.1, it is necessary to determine the peak factor of the floor vibration during the running of the train. As shown in Fig. 16, the vibration acceleration time domain signal of the floor under the passive shock absorber is calculated. The maximum peak value is 2.201 m/s^2 , and the rms value is 0.639 m/s^2 . Therefore, the peak factor of the floor vibration during the running of the train is 3.44, so the estimated vibration dose value (eVDV) is more suitable for the evaluation of human comfort.

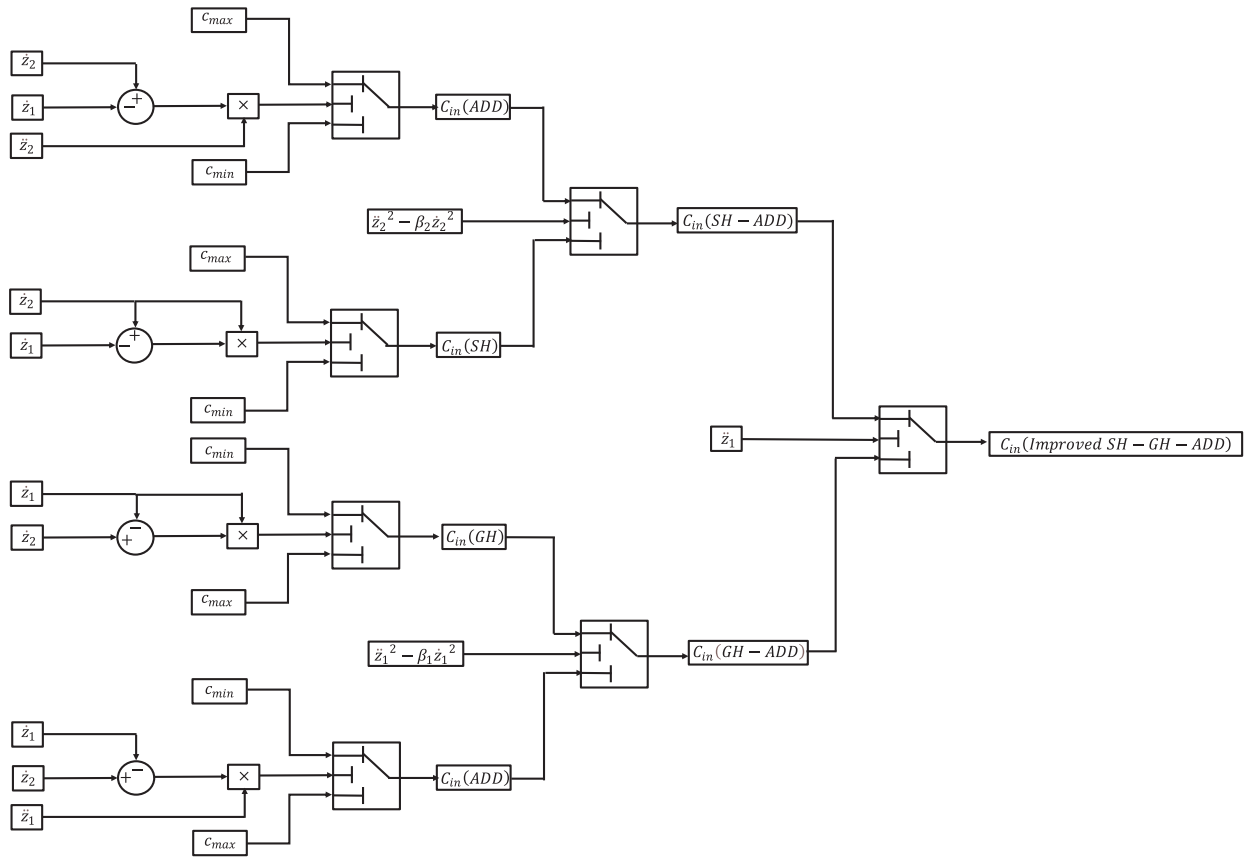


Figure 15: Module schematic based on improved SH-GH-ADD control strategy

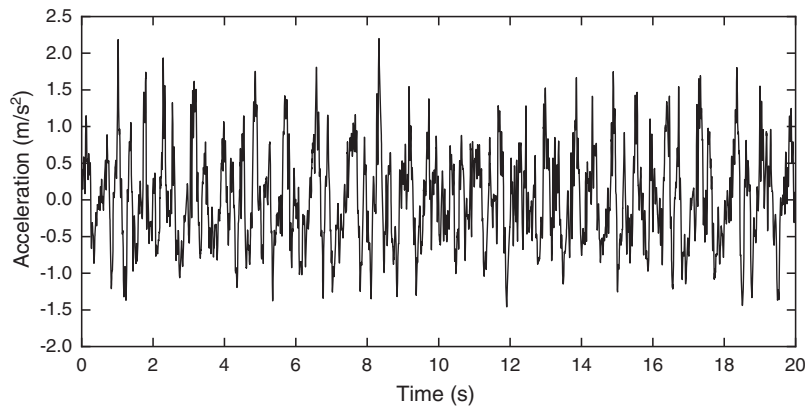


Figure 16: Acceleration response of floor under passive shock absorber

In order to fully analyze the frequency range of human comfort adaptation (0.5~12.5 Hz), 0.5 Hz in ISO2631-1:1997 is used as the center frequency of 1/3 frequency doubling, and its lower limit frequency is 0.45; 12.5 Hz is the center frequency of 1/3 frequency doubling, and its upper limit frequency is 14 Hz. In order to characterize the daily occupational vibration exposure, the frequency-weighted acceleration a_w in the frequency range of 0.45–14 Hz is calculated according to the formula of Eq. (3) with 8 h as the time period T, and the estimated vibration dose values under different control strategies are calculated by

Eq. (2). Through simulation, the floor acceleration under various control strategies in the frequency range of 0~14 Hz is shown in Fig. 17, and the estimated vibration dose value under different control strategies is shown in Table 4.

As shown in Table 4, the eVDV under various control strategies in the range of 0.45~14 Hz have been improved compared with the passive suspension. Among them, the Improved SH-GH-ADD control has the most obvious effect on the comfort of the human body, which can effectively reduce the fatigue effect of the human body.

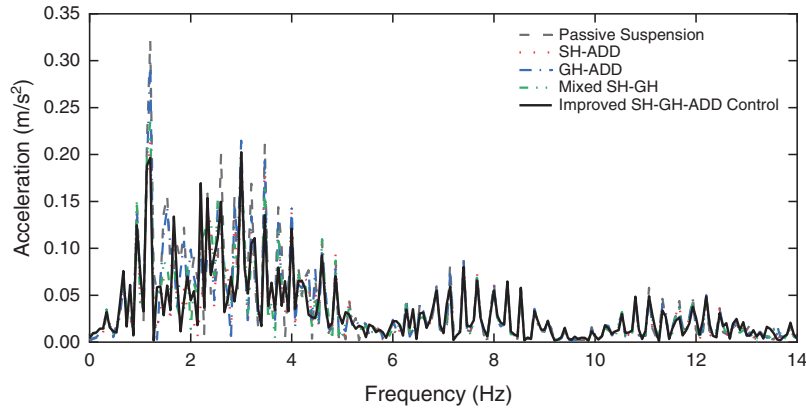


Figure 17: Acceleration frequency domain response of the floor

Table 4: Comparison of estimated vibration dose values under different control strategies

Control strategy	a_w (m/s ²)	eVDV (m/s ^{1.75})
Passive suspension	0.197	3.59
SH-ADD	0.167	3.05
GH-ADD	0.185	3.40
Mixed SH-GH	0.173	3.15
Improved SH-GH-ADD control	0.165	3.01

5.2 Vehicle Ride Comfort Analysis

According to the simulation analysis, the vibration displacement and acceleration of the lead-car floor of various control strategies is shown in Figs. 18 and 19. The floor vibration displacement of the lead-car with various control strategies is shown in Table 5. The evaluation indexes of different control strategies are calculated by the vehicle ride comfort evaluation index, as shown in Table 6.

It can be seen from Tables 6 and 7 that the weighted rms displacement, acceleration and equivalent mean value L_{aw} of the seat under various control strategies are improved compared with the passive suspension. Among them, the Improved SH-GH-ADD control has the most improvement rate on the ride comfort of the vehicle, from the subjective feelings of people from some discomfort to no discomfort.

5.3 Road Friendliness Analysis

Through simulation analysis, the tire dynamic load under various control strategies is shown in Figs. 20–23 and the root mean square value of tire dynamic load is shown in Table 6.

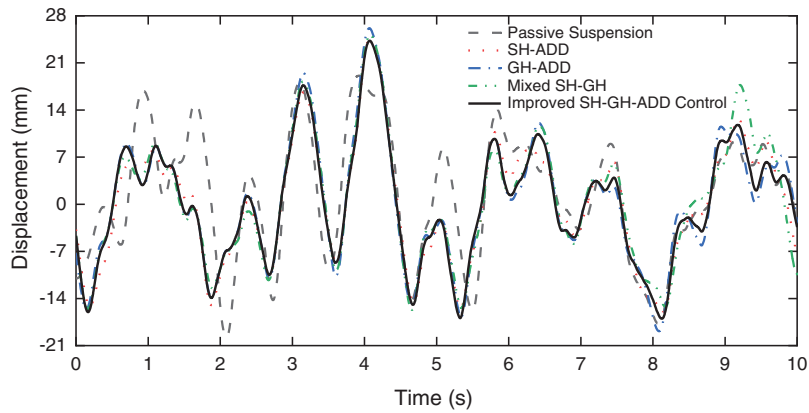


Figure 18: Time domain signal of floor vibration displacement

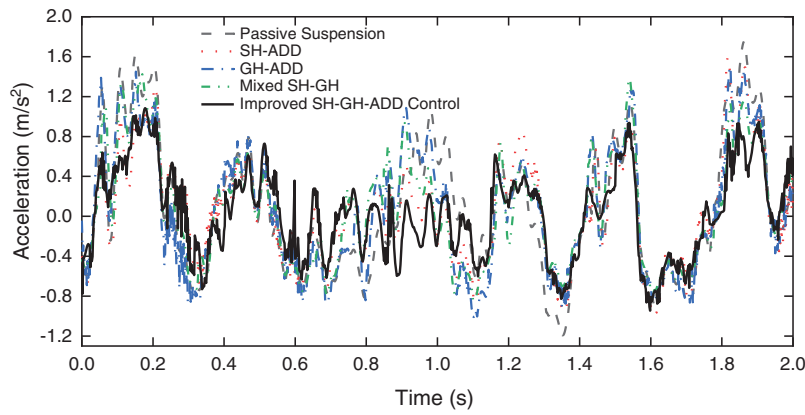


Figure 19: Time domain signal of floor vibration acceleration

Table 5: Comparison of floor vibration displacement with various control strategies

Control strategy	Weighted rms displacement of the seat (mm)	Increase percentage
Passive suspension	9.43	-
SH-ADD	8.81	6.61%
GH-ADD	9.12	3.28%
Mixed SH-GH	9.10	3.51%
Improved SH-GH-ADD control	8.69	7.88%

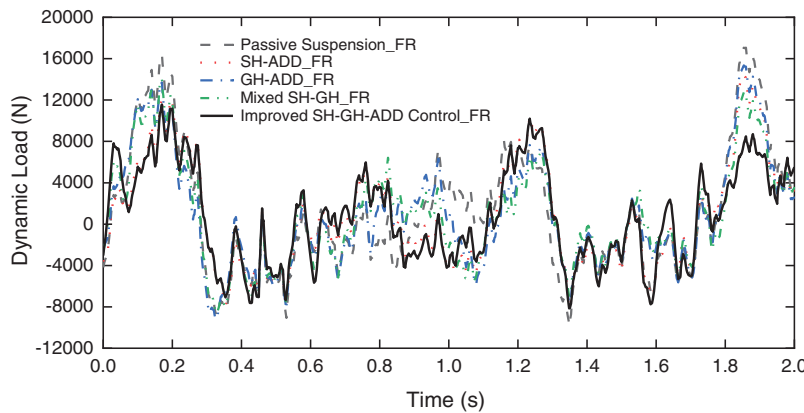
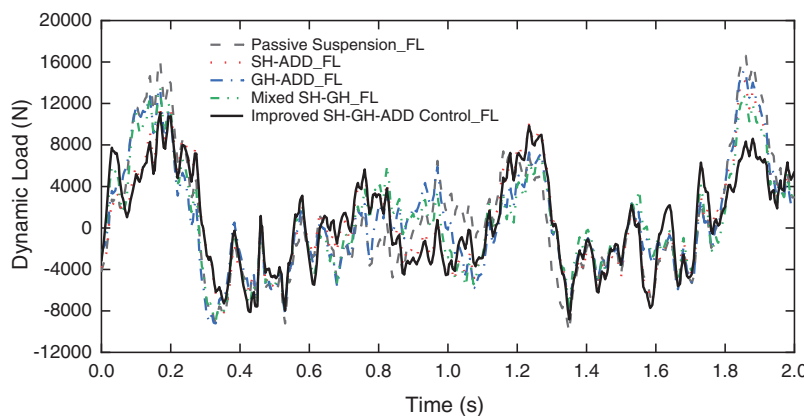
Table 6: Comparison of ride comfort evaluation indexes under different control strategies

Control strategy	Weighted rms acceleration of the seat (m/s^2)	L_{aw}
Passive suspension	0.480	113.632
SH-ADD	0.385	111.709
GH-ADD	0.446	112.990
Mixed SH-GH	0.399	112.019
Improved SH-GH-ADD control	0.315	109.965

Table 7: Comparison of root mean square values of tire dynamic load

Control strategy	Dynamic load of right front tire/N	Dynamic load of left front tire/N	Dynamic load of right rear tire/N	Dynamic load of left rear tire/N
Passive suspension	6130.37	5986.38	4212.19	4286.77
SH-ADD	5189.49(15.35%)	5124.45(14.40%)	3993.22(5.20%)	4010.30(6.45%)
GH-ADD	5334.68(12.98%)	5252.87(12.25%)	4269.64(-1.37%)	4307.22(-0.48%)
Mixed SH-GH	5007.03(18.32%)	4927.51(17.69%)	3953.55(6.14%)	3973.28(7.31%)
Improved SH-GH-ADD control	4669.01(23.84%)	4597.94(23.19%)	3512.42(16.61%)	3537.48(17.48%)

Note: The values in brackets are the promotion rate of different tire dynamic loads under various control strategies.

**Figure 20:** Dynamic load of right front tire**Figure 21:** Dynamic load of left front tire

From Table 7, it can be seen that the root mean square value of tire dynamic load under various control strategies is improved compared with that of passive suspension. Among them, Improved SH-GH-ADD control draws on the advantages of SH-ADD control and GH-ADD control, which greatly improves the tire dynamic load of the front and rear axles. Among the four control strategies, the proposed control strategy has obvious optimization effect on tire dynamic load.

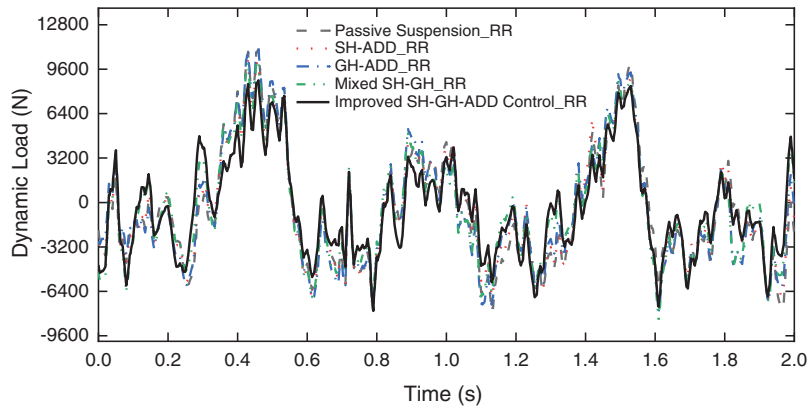


Figure 22: Dynamic load of right rear tire

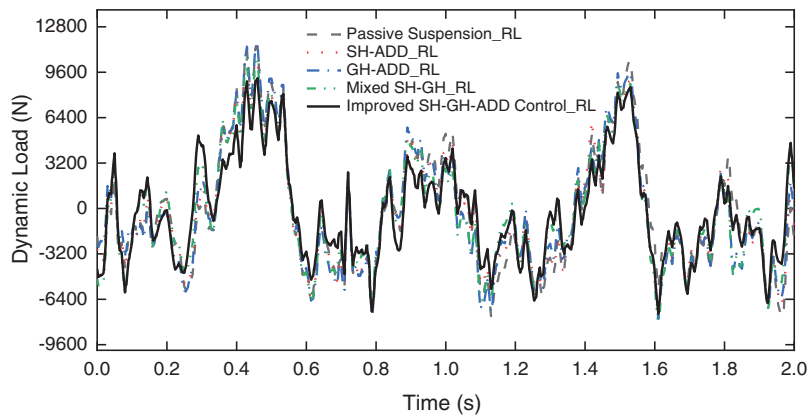


Figure 23: Dynamic load of left rear tire

The virtual track train is driven by automatic tracking, and its load repeatedly acts on the road surface. Through the investigation, the daily running time of the virtual track train is 6:00~22:00, and the statistical results of the number of times that the virtual track train tire passes through a section are collected [1], as shown in Table 8.

Table 8: Statistics of the number of passes through a section

1 day	1 year	5 years	10 years
288	105120	525600	1051200

Since the road friendliness evaluation index considers the vehicle axle load, the value of the P_d tire dynamic load in this paper is the average of the front axle and the rear axle. The road friendliness indexes of different control strategies at different speeds are calculated by the road friendliness evaluation index, as shown in Table 9.

Table 9: Pavement permanent deformation under different control strategies

Year/(times)	Control strategy	Permanent deformation	Increase percentage
1 year/105120	Passive suspension	3.98	-
	SH-ADD	3.87	2.86%
	GH-ADD	3.91	1.81%
	Mixed SH-GH	3.85	4.62%
	Improved SH-GH-ADD control	3.77	5.28%
5 years/525600	Passive suspension	14.74	-
	SH-ADD	14.32	2.86%
	GH-ADD	14.47	1.81%
	Mixed SH-GH	14.24	4.62%
	Improved SH-GH-ADD control	13.96	5.28%
10 years/1051200	Passive suspension	25.90	-
	SH-ADD	25.16	2.86%
	GH-ADD	25.43	1.81%
	Mixed SH-GH	25.01	4.62%
	Improved SH-GH-ADD control	24.53	5.28%

Through the permanent damage prediction equation of the road surface, the permanent damage of the vehicle to the road in different years is predicted. As shown in Table 9, the permanent deformation of the road surface under various control strategies is improved compared with the passive suspension. Among them, the improved SH-GH-ADD control has the least damage to the road surface, indicating that the control has better road friendliness than other controls.

6 Conclusion

This paper proposes an improved SH-GH-ADD control strategy for enhancing human comfort, vehicle ride comfort, and road friendliness. Firstly, the virtual rail train's human comfort, vehicle ride comfort, and road friendliness are evaluated from multiple perspectives using the human-vehicle-road friendliness approach. Secondly, the multibody dynamics model of the virtual rail train is experimentally verified, demonstrating its high validity and correctness. This verification also confirms the reliability and practical application value of simulation analysis based on the model to some extent. Next, the advantages and disadvantages of SH-ADD, GH-ADD, and Mixed SH-GH control strategies are compared and analyzed. To reduce the vehicle's force on the road surface and suppress body vibration simultaneously, an improved SH-GH-ADD control strategy based on unsprung mass acceleration is proposed. This strategy combines the benefits of SH-ADD and GH-ADD control strategies. Finally, using the hub-driven virtual rail train dynamics model, the correctness and effectiveness of the improved SH-GH-ADD control strategy are verified by taking human comfort, vehicle ride comfort, and road friendliness as evaluation indices. The results indicate that SH-ADD, GH-ADD, Mixed SH-GH, and improved SH-GH-ADD control strategies all improve the human-vehicle-road friendliness of the virtual rail train, with the improved SH-GH-ADD control strategy having the most significant impact.

Acknowledgement: The authors would like to acknowledge the support from the Sichuan Provincial Natural Science Foundation and the facilities provided by the Institute of Energy and Power Research at Southwest Jiaotong University for the experimental research.

Funding Statement: This research was funded by Natural Science Foundation of Sichuan Province (2023NSFSC0395), the Sichuan Science and Technology Program (2022ZH CG0061), the SWJTU Science and Technology Innovation Project (2682022CX008).

Author Contributions: Writing-original draft: Yangyang Bao; supervision, funding acquisition: Mingliang Yang, Weiping Ding; methodology: Haibo Huang; writing—review and editing: Liyuan Liu, Honglin Zhu. All authors reviewed the results and approved the final version of the manuscript.

Availability of Data and Materials: The data used to support the findings of this study are available from the corresponding author upon request.

Conflicts of Interest: The authors declare that they have no conflicts of interest to report regarding the present study.

References

1. Wang, C., Zhang, J., Zhou, H., Lu, H. (2021). Dynamic response and permanent deformation analysis of asphalt pavement under the virtual rail train. *Journal of Tongji University (Natural Science)*, 49(1), 60–66. <https://doi.org/10.11908/j.issn.0253-374x.20274>
2. Du, H., Zhang, N., Fazel, N. (2011). Robust control of vehicle electrorheological suspension subject to measurement noises. *Vehicle System Dynamics*, 49(1–2), 257–275. <https://doi.org/10.1080/00423110903288336>
3. Nguyen, D. N., Nguyen, T. A. (2022). A novel hybrid control algorithm sliding mode-PID for the active suspension system with state multivariable. *Complex*, 2022, 1–14. <https://doi.org/10.1155/2022/9527384>
4. Yokoyama, M., Hedrick, J. K., Toyama, S. (2001). A model following sliding mode controller for semi-active suspension systems with MR dampers. *Proceedings of the 2001 American Control Conference*, pp. 2652–2657. Arlington, VA, USA. <https://doi.org/10.1109/ACC.2001.946276>
5. Huang, X., Huang, H., Peng, Y., Ralescu, A. L., Sun, S. (2023). Dissipativity-based adaptive integral sliding mode control of Takagi-Sugeno fuzzy descriptor systems. *IET Control Theory & Applications*, 17(1), 53–73.
6. Nguyen, T. A. (2023). A novel approach with a fuzzy sliding mode proportional integral control algorithm tuned by fuzzy method (FSMPIF). *Scientific Reports*, 13(1), 7327. <https://doi.org/10.1038/s41598-023-34455-7>
7. Nguyen, D. N., Nguyen, T. A. (2023). Proposing an original control algorithm for the active suspension system to improve vehicle vibration: Adaptive fuzzy sliding mode proportional-integral-derivative tuned by the fuzzy (AFSPIDF). *Heliyon*, 9(3), e14210. <https://doi.org/10.1016/j.heliyon.2023.e14210>
8. Karnopp, D., Crosby, M. J., Harwood, R. A. (1974). Vibration control using semi-active force generators. *Journal of Engineering for Industry*, 96(2), 619–626. <https://doi.org/10.1115/1.3438373>
9. Valášek, M., Novák, M., Šika, Z., Vaculín, O. (1997). Extended ground-hook-new concept of semi-active control of truck's suspension. *Vehicle System Dynamics*, 27(5–6), 289–303. <https://doi.org/10.1080/00423119708969333>
10. Savaresi, S. M., Silani, E., Bittanti, S. (2005). Acceleration-driven-damper (ADD): An optimal control algorithm for comfort-oriented semiactive suspensions. *Journal of Dynamic Systems Measurement & Control*, 127(2). <https://doi.org/10.1115/1.1898241>
11. Savaresi, S. M., Spelta, C. (2007). Mixed sky-hook and ADD: Approaching the filtering limits of a semi-active suspension. *Journal of Dynamic Systems, Measurement, and Control*, 129(4), 382–392. <https://doi.org/10.1115/1.2745846>
12. Wang, Y. (2020). *Research on control strategy of semi-active suspension considering phase compensation* (Ph.D. Thesis). Jilin University, China.

13. Guo, K., Sui, J., Guo, Y. (2013). Semi-active control method for a high-speed railway vehicle lateral damper based on skyhook and groundhook hybrid damping. *Journal of Vibration and Shock*, 32(2), 18–23. <https://doi.org/10.13465/j.cnki.jvs.2013.02.028>
14. Huang, H., Lim, T. C., Wu, J., Ding, W., Pang, J. (2023). Multitarget prediction and optimization of pure electric vehicle tire/road airborne noise sound quality based on a knowledge and data-driven method. *Mechanical Systems and Signal Processing*, 197, 110361. <https://doi.org/10.1016/j.ymssp.2023.110361>
15. Zhao, L., He, Q. (1992). Human response to low frequency vibration below 1.0 Hz. *Automotive Engineering*, 1992(2), 65–69+80. <https://doi.org/10.19562/j.chinasae.qcgc.1992.02.001>
16. Huang, H., Huang, X., Ding, W., Yang, M., Yu, X. (2022). Vehicle vibro-acoustical comfort optimization using a multi-objective interval analysis method. *Expert Systems with Applications*, 213, 119001. <https://doi.org/10.1016/j.eswa.2022.119001>
17. Dong, S., Zhu, Y. (2004). Effects of environmental vibration on man. *Noise and Vibration Control*, 24(3), 22–25. <https://doi.org/10.3969/j.issn.1006-1355.2004.03.007>
18. Huang, H., Huang, X., Ding, W., Zhang, S., Pang, J. (2023). Optimization of electric vehicle sound package based on LSTM with an adaptive learning rate forest and multiple-level multiple-object method. *Mechanical Systems and Signal Processing*, 187, 109932. <https://doi.org/10.1016/j.ymssp.2022.109932>
19. Yu, Z. (2018). *Automobile theory*. 6th edition. Beijing, China: Mechanical Industry Press.
20. Duarte, M. L., Araújo, P. A., Horta, F. C., Vecchio, S. D., Carvalho, L. A. (2018). Correlation between weighted acceleration, vibration dose value and exposure time on whole body vibration comfort levels evaluation. *Safety Science*, 218–224. <https://doi.org/10.1016/j.ssci.2017.11.008>
21. Yang, Y., Liu, P., Yin, J. (2014). Research on assessment of fourth power vibration dose value in environmental vibration caused by metro. *21st International Congress on Sound and Vibration 2014: ICSV 21*, pp. 1092–1099. Beijing, China.
22. Mechanical vibration and shock-evaluation of human exposure to whole-body vibration–Part 1: General requirements.
23. Chen, J. (2008). *MSC.ADAMS technology and engineering analysis example*. Beijing, China: China Water & Power Press.
24. Theyse, H. L. (1997). Mechanistic-empirical modeling of the permanent deformation of unbound pavement layers. *8th International Conference on Asphalt Pavements*, vol. 2, pp. 1579–1594. Seattle, USA.
25. Liu, B., Yao, Z. (2002). Introduction about revision of specifications of cement concrete pavement design for highway. *Highway*, 1–7. <https://doi.org/10.3969/j.issn.0451-0712.2002.08.001>
26. Zhang, X., Ding, J. (2021). Firefly algorithm for multi-body system dynamics differential-algebraic equations. *Journal of Dynamics and Control*, 19(2), 85–90. <https://doi.org/10.6052/1672-6553-2020-113>
27. Zhang, X. (2020). *Intelligent algorithm for solving differential-algebraic equations of multibody system dynamics*. Qingdao, China: Qingdao University. <https://doi.org/10.27262/d.cnki.gqdau.2020.001759>
28. Kan, Z., Peng, H., Chen, B. (2017). Rigid body system dynamic with the accurate jacobian matrix of spring-damper-actuator. *Chinese Journal of Theoretical and Applied Mechanics*, 49(5), 1103–1114. <https://doi.org/10.6052/0459-1879-17-030>
29. Savaresi, S. M. (2010). Classical control for semi-active suspension system. *Semi-Active Suspension Control Design for Vehicles*, 107–120. <https://doi.org/10.1016/b978-0-08-096678-6.00006-7>
30. Fan, D., Dai, P., Yang, M., Jia, W., Jia, X. et al. (2022). Research on maglev vibration isolation technology for vehicle road noise control. *SAE International Journal of Vehicle Dynamics, Stability, and NVH*, 6(3), 233–245.
31. Jin, T., Liu, Z., Sun, S., Ren, Z., Deng, L. et al. (2020). Development and evaluation of a versatile semi-active suspension system for high-speed railway vehicles. *Mechanical Systems and Signal Processing*, 135, 106338. <https://doi.org/10.1016/j.ymssp.2019.106338>
32. Yan, W., Dong, D., Wang, W., Wu, C., Liu, Z. et al. (2011). On fuzzy control strategy of nonlinear semi-active suspension system. *Control Engineering of China*. <https://doi.org/10.14107/j.cnki.kzgc.2011.06.010>